Inorganic Chemistry

Article

pubs.acs.org/IC

TCM Active Ingredient Oxoglaucine Metal Complexes: Crystal Structure, Cytotoxicity, and Interaction with DNA

Zhen-Feng Chen,* Yan-Fang Shi, Yan-Cheng Liu, Xue Hong, Bo Geng, Yan Peng, and Hong Liang*

State Key Laboratory Cultivation Base for the Chemistry and Molecular Engineering of Medicinal Resources, School of Chemistry & Chemical Engineering, Guangxi Normal University, Guilin, 541004, China

Supporting Information

ABSTRACT: The alkaloid oxoglaucine (OG), which is a bioactive component from traditional Chinese medicine (TCM), was synthesized by a two-step reaction and used as the ligand to react with transition metal salts to give four complexes: $[OGH][AuCl_4]\cdot DMSO$ (**1**), $[Zn(OG)_2(H_2O)_2](NO_3)_2$ (**2**), $[Co(OG)_2(H_2O)_2](ClO_4)_2$ (**3**), and $[Mn(OG)_2(H_2O)_2](ClO_4)_2$ (**4**). The crystal structures of the metal complexes were confirmed by single crystal X-ray diffraction. Complex **1** is an ionic compound consisting of a charged ligand $[OGH]^+$ and a gold complex $[AuCl_4]^-$. Complexes **2**−**4** all have similar structures (inner-spheres), that is, octahedral geometry with two OG coordinating to one metal center and two aqua ligands occupying the two apical positions of the octahedron, and two NO_3^- or ClO_4^- as counteranions in the outer-sphere. The complexation of OG to metal ion was confirmed by ESI-MS, capillary electrophoresis and fluorescence polarization. The in vitro cytotoxicity of these complexes toward a various tumor cell lines was assayed by the MTT method. The results showed that most of these metal−oxoglaucine complexes exhibited enhanced cytotoxicity compared with oxoglaucine and the corresponding metal salts, with IC_{50} values ranging from 1.4 to 32.7 μM for sensitive cancer cells, which clearly implied a positive synergistic effect. Moreover, these complexes appeared to be selectively active against certain cell lines. The interactions of oxoglaucine and its metal complexes with DNA and topoisomerase I were investigated by UV−vis, fluorescence, CD spectroscopy, viscosity, and agarose gel electrophoresis, and the results indicated that these OG−metal complexes interact with DNA mainly via intercalation. Complexes **2**−**4** are metallointercalators, but complex **1** is not. These metal complexes could effectively inhibit topoisomerase I even at low concentration. Cell cycle analysis revealed that **1**−**3** caused S-phase cell arrest.

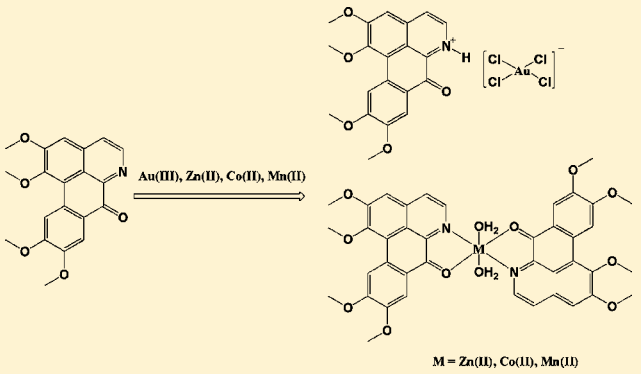

INTRODUCTION

Since the successful use of cisplatin and related platinum complexes as anticancer agents, developing other transition metal complexes as active anticancer agents with better efficiency and new mechanisms of action has become a central research theme in bioinorganic chemistry.[1−5] The discovery of nonplatinum metal-based anticancer complexes with potent anticancer activity, such as gold(III),[6] zinc(II),[7] cobalt(II)/(III),[8] and manganese(II)[9] complexes, has been extensively investigated during the past two decades. Recently some new coordination compounds based on traditional Chinese medicines (TCMs) were found to afford novel potential (pro)drugs.[10,11] Our group previously reported a series of metal complexes bearing liriodenine/plumbagin/matrine ligands as anticancer compounds,[12] and in our continuing research, we now focus on the oxoaporphine−metal complex as anticancer agents. Oxoglaucine (OG, Scheme 1) is an oxoaporphine alkaloid that has been isolated from the overground parts of plants from different families, such as *Annonaceae*,[13,14] *Lauraceae*,[15] *Magnoliaceae*,[16] *Fumariaceae*,[17,18] *Menispermaceae*,[19] and *Papveraceae*.[20,21] It is also commonly found in many traditional Chinese medicines, such as *aquilegia ecalcarata Maxim* (*Ranunculaceae*), which is mainly distributed in the Sichuan and Yunnan provinces of China and used to treat necrotic boils, pustulosis, and other infections.[22] The primary screening results reveal that oxoglaucine possesses strong anticancer activity, for example, against HCT-8 (ED_{50} = 2.85 μM) and KB (ED_{50} = 5.69 μM).[23] In addition, oxoglaucine exhibits other important pharmacological properties including antiplatelet aggregation,[13,24] immunomodulatory activity,[25] amelioration of adjuvant arthritis,[26] anti-inflammatory activity,[27] antifungal activity.[28]

Intercalators are small organic molecules or metal complexes that unwind DNA to π-stack between two neighboring base pairs. Metallointercalators are metal complexes that bear at least one intercalating ligand. Since the preparation of the first platinum metallointercalator by S. J. Lippard and co-workers,[29]

Received: March 4, 2011
Published: February 6, 2012

Scheme 1. Synthesis Route of Oxoglaucine

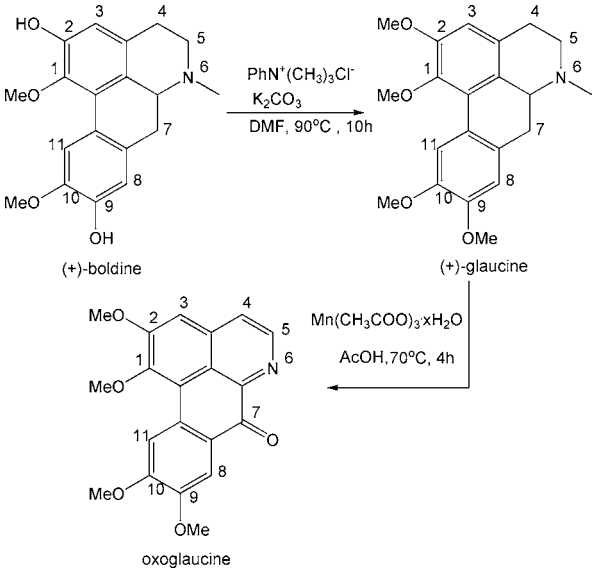

over the past three decades, there has been rising interest on octahedral transition metal complexes as metallointercalator[30] and new dual-function metal complexes that can interact with DNA by both coordination and intercalation,[31] which may have potential diagnostic and therapeutic applications. Because OG is an aromatic planar ligand with N and carbonyl O donors, it can coordinate to metal to form metal intercalator.

We previously noted the potent anticancer activity of the gold(III),[6] zinc(II),[7] cobalt(II)/(III),[8] and manganese(II)[9] complexes with different N/O donor ligands. To explore alkaloid−metal complexes as anticancer agents, we synthesized oxoglaucine and reacted it with the gold(III), zinc(II), cobalt(II) and manganese(II) salts to afford four metal complexes. Herein, we report the synthesis and characterization of oxoglaucine and its metal complexes: [OGH]-$[AuCl_4]$·DMSO (**1**), $[Zn(OG)_2(H_2O)_2](NO_3)_2$ (**2**), $[Co(OG)_2(H_2O)_2](ClO_4)_2$ (**3**), and $[Mn(OG)_2(H_2O)_2](ClO_4)_2$ (**4**). Their cytotoxicity and interactions with DNA and topoisomerase I were also investigated.

EXPERIMENTAL SECTION

Materials. All chemicals, unless otherwise noted, were purchased from Sigma and Alfa Aesar. All materials were used as received without further purification unless noted specifically. Tris-HCl-NaCl (TBS) buffer solution (5 mM Tris, 50 mM NaCl, pH adjusted to 7.35 by titration with hydrochloric acid using a Sartorius PB-10 pH meter, Tris = tri(hydroxymethyl)aminomethane) was prepared using double distilled water. The TBE buffer (1×) and DNA loading buffer (6×) were commercially available. Calf thymus DNA (ct-DNA) was purchased from Sino-American Biotech Co., Ltd. (Beijing). Ct-DNA gave a UV absorbance ratio at 260−280 nm of ~1.85:1, indicating that the DNA was effectively free of protein.[32] The DNA concentration per nucleotide was determined spectrophotometrically by employing a molar absorption coefficient (6600 $M^{-1}cm^{-1}$) at 260 nm.[33] TOPO I was purchased from Sigma. The stock solution of pUC19 plasmid DNA (250 μg/mL) was purchased from Takara Biotech Co., Ltd.

Instrumentation. Infrared spectra were obtained on a Perkin-Elmer FT-IR Spectrometer. ^1H NMR and ^{13}C NMR spectra were recorded on a Bruker AV-500 NMR spectrometer with $(CD_3)_2SO$ as solvent. Elemental analyses (C, H, and N) were carried out on a PerkinElmer Series II CHNS/O 2400 elemental analyzer. ESI-MS spectra for the characterization of complexes **1**−**4** were performed on Thermofisher Scientific Exactive LC-MS Spectrometer. ESI-MS spectra for the stability studies on the complexes **1**−**4** were recorded on a Bruker HCT Electrospray Ionization Mass Spectrometer. Capillary electrophoresis was recorded on Agilent HP3D High-performance capillary electrophoresis. Fluorescence polarization was performed on Horiba Jobin Jvon FL3-P-TCSPC Time-Resolved Fluorescence spectrometer. UV−vis absorption titration was performed on a Varian Cary100 UV−visible spectrophotometer. Fluorescence emission titration was performed on a Shimadzu RF-5301/PC spectrofluorophotometer. The Circular dichroic spectra of DNA in the region between 200 and 400 nm were obtained by using a JASCO J-810 automatic recording spectropolarimeter operating at 25 °C. Viscosity of DNA solution was measured on a Brookfield LVDV-II + Pro digital viscometer equipped with a ULV adapter, as well as a Brookfield TC-502D digital controlled circulating bath for constant temperature.

Caution! *Perchlorate complexes are potentially explosive. The experiments were carried out in an isolated room and the operator must be protected with blast shield and other necessary equipments. The perchlorate complexes should be prepared only in small amount and handled with extreme care.*

Synthesis of (+)-Glaucine. To a solution of (+)-boldine (1.80 g, 5.498 mmol) and trimethylphenylammonium chloride (3.303 g, 19.24 mmol) in dry DMF (100 mL) was added anhydrous K_2CO_3 (3.78 g, 27.292 mmol), and the suspension was heated to 90 °C under N_2 for 16 h. After removal of the organic solvent by vacuum distillation, the residue was dissolved in $CHCl_3$ and washed with 5% sodium hydroxide solution (100 mL × 2) followed by H_2O (100 mL × 3). The organic layer was dried over anhydrous sodium sulfate and concentrated under reduced pressure. The residue was purified by silica gel chromatography using gradient elution with $CHCl_3$−CH_3OH (200:1 to 30:1) to afford (+)-glaucine (1.1 g, 60%). mp: 112−114 °C. ^1H NMR ($CDCl_3$, 500 MHz): δ 8.07 (1H, s, H-11), 6.74 (1H, s, H-8), 6.55 (1H, s, H-3), 3.90 (3H, s, 9-OMe), 3.89 (3H, s, 10-OMe), 3.85 (3H, s, 2-OMe), 3.64 (3H, s, 1-OMe), 2.53 (s, N-Me). APCI-MS: [M + H] 356.

Synthesis of Oxoglaucine. To a solution of glaucine (1.18 g, 3.30 mmol) in acetic acid (50 mL) was added manganese(III) acetate hydrate (26.20 mmol), and the mixture was stirred at 70 °C for 2 h. After the completion of the reaction (monitored by TLC), acetic acid was distilled off under high vacuum, and the residue was dissolved in chloroform (100 mL) and washed with saturated $NaHCO_3$ solution (50 mL), followed by water (3 × 50 mL). The organic layer was dried over anhydrous sodium sulfate and then concentrated under reduced pressure. The residue was purified by silica gel chromatography using gradient elution of $CHCl_3/CH_3OH$ (200:0 to 200:1) to afford oxoglaucine as yellow fine needles (0.285 g, 25%). The crystals of oxoglaucine suitable for single-crystal X-ray diffraction analysis were obtained by recrystallization from $CHCl_3/CH_3OH$ at room temperature. mp: 196−198 °C. IR(KBr, cm^{-1}): 2938 (m, Ar−H), 1647 (s, C═O), 1594(s), 1571(s), 1510 (m), 1463(s), 1277(m, C−O), 1243(s), 1068(m, C−N). ^1H NMR ($CDCl_3$, δ_H,500 MHz): δ4.02(s, 3H, OCH_3), 4.06(s, 6H, 2 × OCH_3), 4.0(s, 3H, OCH_3), 7.15(s, 1H, C_3−H), 7.72d, 1H, J = 5.2 Hz, C_4−H), 7.99(s, 1H, C_8−H), 8.76(s, 1H, C_{11}−H), 8.86(d, 1H, J = 5.2 Hz, C_5−H). ^{13}C NMR($CDCl_3$, δ_C,125 MHz): 181.2, 157.2, 152.7, 151.3, 148.5, 145.6, 145.0, 136.2, 128.8, 126.4, 123.7, 120.5, 118.9, 110.2, 109.5, 105.3, 60.5, 56.7, 56.7, 56.7.

General Procedure for the Synthesis of Complexes 1−4. To a mixture of the corresponding metal salt, oxoglaucine, methanol (1 mL), and $CHCl_3$ (0.25 mL) was placed in a thick Pyrex tube (~20 cm long). The mixture was frozen by liquid N_2 and evacuated under vacuum, then sealed with a torch, warmed to room temperature, and heated at 80 °C for a few days to give the corresponding block crystals of the complexes **1**−**4** suitable for X-ray diffraction analysis.

[OGH][$AuCl_4$]·DMSO (1). $HAuCl_4·4H_2O$ (0.041 g, 0.1 mmol), oxoglaucine (0.0351 g, 0.1 mmol). Yield: 0.050 g, 65%. Anal. Found (%): C, 34.32; H, 3.12; N, 1.86. Calcd for $C_{22}H_{24}AuCl_4NO_6S$: 34.35; H, 3.14; N, 1.82. Main IR (KBr, cm^{-1}) peaks: 3422 m (−NH), 3080 m (Ar−H), 1657s (C═O), 1622s, 1588s (C═C), 1477s, 1287 m (C−O), 1254s, 1065s (C−N). ^1H NMR(DMSO-d_6, δ_H, 500 MHz):

dx.doi.org/10.1021/ic200443p | Inorg. Chem. 2012, 51, 1998−2009

Table 1. Crystal Data and Structure Refinement Details for OG and Complexes 1−4

formula	$C_{20}H_{17}NO_5$	$C_{22}H_{24}AuCl_4NO_6S$	$C_{40}H_{38}N_4O_{18}Zn$	$C_{40}H_{38}Cl_2CoN_2O_{20}$	$C_{40}H_{38}Cl_2MnN_2O_{20}$
fw	351.35	769.25	928.11	996.55	992.56
T, K	296(2)	296(2)	293(2)	296(2)	223(2)
cryst syst	monoclinic	monoclinic	triclinic	triclinic	triclinic
space group	$P2(1)/n$	$P2(1)/n$	$P\bar{1}$	$P\bar{1}$	$P\bar{1}$
a, Å	7.1197(15)	8.5115(6)	8.323(6)	8.6032(16)	8.6702(6)
b, Å	15.374(3)	12.3968(9)	11.010(7)	11.174(2)	11.1589(6)
c, Å	15.031(3)	25.1060(18)	11.838(8)	12.212(2)	12.2521(6)
α, deg	90	90	101.369(12)	65.314(2)	63.838(8)
β, deg	92.461(3)	96.1080(10)	104.335(16)	74.206(2)	74.356(9)
γ, deg	90	90	104.810(8)	78.120(2)	77.682(10)
V, Å^3	1643.7(6)	2634.0(3)	976.1(11)	1020.7(3)	1018.40
Z	4	4	1	1	1
D_c, g cm^{-3}	1.420	1.937	1.579	1.621	1.618
μ, mm^{-1}	0.103	6.109	0.718	0.641	0.545
GOF on F^2	1.009	1.024	1.070	1.040	1.056
reflns (collected/unique)	8193/2929	12869/4624	9225/3549	5126/3563	8788/3757
R_{int}	0.0657	0.0255	0.0762	0.0235	0.0354
$R_1{}^a$ ($I > 2\sigma(I)$)	0.0649	0.0295	0.0912	0.0640	0.0514
$R_2{}^b$ ($I > 2\sigma(I)$)	0.2230	0.0692	0.2429	0.2055	0.1314

$^aR_1 = \Sigma\ ||F_o| - |F_c||/\Sigma|F_o|$. $^bR_2 = [\Sigma w(F_o^2 - F_c^2)^2/\Sigma w(F_o^2)^2]^{1/2}$.

δ3.794(s, 3H, OCH_3), 3.848(s, 3H, OCH_3), 4.041(s, 6H, 2 × OCH_3), 7.269 (s, 2H, C_3−H), 7.401(s, 2H, C_{11}−H), 8.187(d, 2H, J =5.2 Hz, C_4−H), 8.384(d, 2H, J =5.2 Hz, C_8−H), 8.462(s, 2H, C_5−H). ^{13}C NMR(DMSO-d_6, δ_C, 125 MHz): δ 206.8, 173.8, 158.7, 158.1, 154.8, 148.3, 139.4, 133.2, 132.1, 131.0, 124.5, 122.8, 120.7, 109.8, 107.6, 107.5, 105.3, 57.4, 55.9, 55.7, 40.0. ESI-MS: m/z 338.84 $[AuCl_4]^-$, 352.12 $[OGH]^+$.

$[Zn(OG)_2(H_2O)_2](NO_3)_2$ (**2**). $Zn(NO_3)_2{\cdot}6H_2O$ (0.030 g, 0.1 mmol), oxoglaucine (0.070 g, 0.2 mmol). Yield: 0.060 g, 65%. Anal. Found (%): C, 51.72; H, 4.18; N, 6.12. Calcd for $C_{40}H_{38}N_4O_{18}Zn$: 51.76; H, 4.13; N, 6.04. Main IR (KBr, cm^{-1}): 3443s (−OH), 2946 m (Ar−H), 1620w (C═O), 1574 m (C═C), 1508 m 1469 m, 1384s (NO_3^-), 1283 m (C−O), 1260 m, 1023(m) (C−N). ^{1}H NMR(DMSO-d_6, δ_H, 500 MHz): δ3.807(s, 6H, OCH_3), 3.970(s, 12H, 2 × OCH_3), 4.01(s, 6H, OCH_3), 8.307 (s, 2H, C_3−H), 8.409(s, 2H, C_{11}−H), 8.881(d, 2H, J = 5.2 Hz, C_4−H), 8.927(d, 2H, J = 5.2 Hz, C_8−H), 9.184 (s, 2H, C_5−H). ^{13}C NMR(DMSO-d_6, δ_C, 125 MHz): δ 206.9, 188.7, 157.9, 156.6, 154.9, 150.2, 148.8, 146.4, 134.9, 130.3, 126.7, 123.4, 121.6, 117.5, 110.5, 108.9, 61.6, 57.3, 56.6, 56.2, 45.9, 44.9. ESI-MS: m/z 828.14 $[Zn(OG)_2 + NO_3]^+$, 558.63 $[Zn(OG)_3]^{2+}$, 383.07 $[Zn(OG)_2]^{2+}$.

$[Co(OG)_2(H_2O)_2](ClO_4)_2$ (**3**). $Co(ClO_4)_2{\cdot}6H_2O$ (0.037 g, 0.1 mmol), oxoglaucine (0.070 g, 0.2 mmol). Yield: 0.068 g, 68%. Anal. Found (%): C, 48.28; H, 3.81; N, 2.89. Calcd for $C_{40}H_{38}Cl_2CoN_2O_{20}$: 48.21; H, 3.84; N, 2.81. Main IR (KBr, cm^{-1}): 3410s (−OH), 2846 m (Ar−H), 1641 m (C═O), 1591 m (C═C), 1571 m, 1508s, 1283 m (C−O), 1260 m, 1109s (ClO_4^-), 1008 m (C−N). ESI-MS: m/z 860.10 $[Co(OG)_2 + ClO_4]^+$, 556.13 $[Co(OG)_3]^{2+}$, 380.58 $[Co(OG)_2]^{2+}$.

$[Mn(OG)_2(H_2O)_2](ClO_4)_2$ (**4**). $Mn(ClO_4)_2{\cdot}6H_2O$ (0.036 g, 0.1 mmol), oxoglaucine (0.070 g, 0.2 mmol). Yield: 0.056 g, 56%. Anal. Found (%): C, 48.46; H, 3.81; N, 2.85. Calcd for $C_{40}H_{38}Cl_2MnN_2O_{20}$: 48.40; H, 3.86; N, 2.82. Main IR (KBr, cm^{-1}): 3423s (−OH), 2942 m (Ar−H), 1643 m (C═O), 1592 m (C═C), 1567 m, 1510s, 1282 m (C−O), 1259 m, 1109s (ClO_4^-), 1008 m (C−N). ESI-MS: m/z 856.11 $[Mn(OG)_2 + ClO_4]^+$, 554.13 $[Mn(OG)_3]^{2+}$, 378.58 $[Mn(OG)_2]^{2+}$.

X-ray Crystallography. Crystal data were collected on a Bruker Smart Apex II CCD or Rigaku Mercury CCD diffractometer equipped with graphite monochromated Mo Kα radiation (λ = 0.71073 Å) at room temperature. Absorption correction were applied by using the multiscan program SADABS.[34] The structures were solved with direct methods and refined using SHELX-97 programs.[35] The non-hydrogen atoms were located in successive difference Fourier synthesis. The final refinement was performed by full-matrix least-squares methods with anisotropic thermal parameters for non-hydrogen atoms on F^2. The hydrogen atoms were added theoretically and riding on the concerned atoms. The crystallographic data and refinement details of the structures are summarized in Tables 1. The selected bond distances and angles for OG, **1**−**4** are given in the corresponding figure captions.

Stability of Complexes 1−4 in Aqueous Solution. Complexes **1**−**4** are soluble at 2 × 10^{-5} M concentration level in the TBS at 25 °C containing 1% DMSO. The kinetic stability of all four complexes was evaluated by UV−vis absorption under this condition. The kinetic

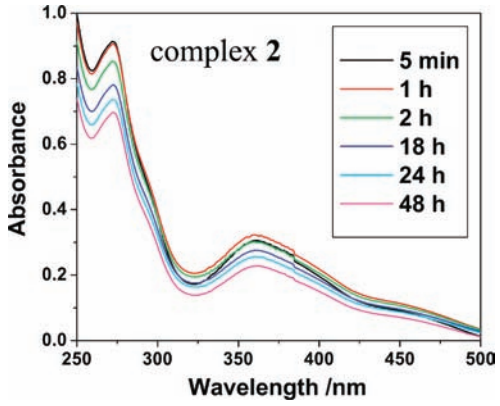

Figure 1. Time-dependent stability studies on complex **2** in TBS monitored by UV−vis absorption spectra.

UV−vis spectra of complex **2** are shown in Figure 1 (for the spectra of OG and complexes **1**, **3** and **4**, see Supporting Information, Figure S1). Complexes **2**, **3**, and **4** showed similar changes in their absorption spectra, most probably because of their similar chemical structures (inner-spheres). Over the time course, the characteristic absorption of each complex all showed hypochromicity but no bathochromic shift. The hypochromicity can be attributed to the gradual formation of aggregates of the complexes in solution, which will decrease their effective concentration for UV−vis absorption.[36] While the UV−vis absorption of OG remained unchanged in 2 h but decreased obviously after 8 and 16 h. No further changes were observed in the UV−vis spectra of complex **1** after 2 h, which suggests a rapid hydrolysis

dx.doi.org/10.1021/ic200443p | Inorg. Chem. 2012, 51, 1998−2009

process and deficient aggregation of **1** within 2 h. Since both OG and its complexes (except for complex **1**) have the UV absorption peaks at same wavelength of 245 and 272 nm, the absence of bathochromic shift cannot unambiguously prove the dissociation of OG ligands from the complexes. As shown in Figure S2 (see Supporting Information), the kinetic ESI-MS spectra (performed on a Bruker HCT Electrospray Ionization Mass Spectrometer) of **1** in TBS indicate that **1** underwent some change while the cation remained unchanged (m/z 352 $[OGH]^+$ and reduction of Au(III) to Au(I), showing the $[AuCl_2]^-$ anion, m/z 267). However, the kinetic ESI-MS spectra of **2**–**4** (see Supporting Information, Figure S2) in TBS are almost unchanged, and mainly contain species $[M(OG)_3]^{2+}$ (m/z 558.6, 556, 554), $[OG_2 + H]^+$ (m/z 703), $[M(OG)_2 + Cl]^+$ (m/z 801, 796, 792), where M = Zn(II), Co(II), Mn(II). These results indicate that the inner-spheres of complexes **2**–**4** are almost stable in TBS, although there exist a small amount of dissociated species and polymeric species ($[M(OG)_3]^{2+}$) in the mass spectrometer, similar to copper(II) complexes with modified indolo[3,2-*c*]quinoline ligands.[37] The ESI-MS results generally agree well with that of UV–vis spectra analysis. In fact, these OG–metal complexes contain various species in TBS that all contribute to the cytotoxicity.

Cytotoxicity Assay. The cell lines BEL7404, SGC7901, HeLa, MCF-7, A549 were obtained from the Shanghai Cell Bank in the Chinese Academy of Sciences. Tumor cell lines were grown in the RPMI-1640 medium supplemented with 10% (v/v) fetal bovine serum, 2 mM glutamine, 100 U/mL penicillin, and 100 U/mL streptomycinin at 37 °C, in a highly humidified atmosphere of 95% air/5% CO_2. The cytotoxicity of MT and the title compounds against BEL7404, SGC7901, HeLa, MCF-7, A549 cell lines were examined by the microculture tetrozolium (MTT) assay.[38] The experiments were carried out using reported procedure.[12] The growth inhibitory rate of treated cells was calculated using the data from three replicate tests as $(OD_{control} - OD_{test})/OD_{control} \times 100\%$. The compounds were incubated with various cell lines for 48 h at five different concentrations of complex dissolved in fresh media; the range of concentrations used is dependent on the complex. The final IC_{50} values were calculated by the Bliss method (n = 5). All tests were independently repeated at least three times.

Cell Cycle Analysis. BEL7404 cell lines were maintained in Dulbecco's modified Eagle's medium with 10% fetal calf serum in 5% CO_2 at 37 °C. Cells were harvested by trypsinization and rinsed with PBS. After centrifugation, the pellet (105–106 cells) was suspended in 1 mL of PBS and kept on ice for 5 min. The cell suspension was then fixed by the dropwise addition of 9 mL precooled (4 °C) 100% ethanol with violent shaking. Fixed samples were kept at 4 °C until use. For staining, cells were centrifuged, resuspended in PBS, digested with 150 mL of RNase A (250 μg/mL), and treated with 150 mL of propidium iodide (PI) (0.15 mM), then incubated for 30 min at 4 °C. PI-positive cells were counted with a FACScan fluorescence-activated cell sorter (FACS). The population of cells in each cell cycle phase was determined using Cell Modi FIT software (Becton Dickinson).

Spectroscopic Studies on DNA Interactions. The synthesized complexes and ligand were dissolved in DMSO to make 2.0 mM stock solutions for DNA binding studies. The 2×10^{-3} M ct-DNA stock solution was stored at 4 °C for no more than 4 days before use. The final working solutions of the complexes for DNA binding studies are diluted in the TBS and the containing DMSO is limited in 1%. In UV–vis absorption spectrometry, the working solutions of OG and the complexes are 20 μM. The ct-DNA stock solution was added 15 μL per scan at a [DNA]/[compound] ratio of 0.5:1 and gradually increased up to a sufficient concentration to achieve saturation for analysis. After each addition, the solution was allowed to incubate for 10 min before the absorption spectra were recorded. The intrinsic binding constant K_b was determined by the following equation: $[DNA]/(\varepsilon_a - \varepsilon_f) = [DNA]/(\varepsilon_a - \varepsilon_f) + 1/[K_b(\varepsilon_a - \varepsilon_f)]$,[32] where [DNA] is the concentration of the DNA, ε_a is the apparent absorption coefficient ($\varepsilon_a = A_{obsd}/[compound]$), ε_f is the extinction coefficient for the free compound, and ε_b is the absorption coefficient of the compound fully bound to DNA. The intrinsic binding constant, K_b, of the compounds are calculated as the ratio of the slope to the Y intercept by linear fitting of $[DNA]/(\varepsilon_a - \varepsilon_f)$ with [DNA] from the above equation. The absolute values of K_b are presented in the inset of each linear fitting plot.

In the CD absorption spectrometry, the working solution of each sample was prepared by using 1×10^{-4} M DNA and titrating the complexes into the DNA solution stepwise with the [DNA]/[compound] ratio ranging from 10:0.5 to 10:5. The working solution was incubated for 10 min after each addition and then its CD spectrum was recorded at 100 nm/min scan rate. The CD signals of the TBS were subtracted as the background. A solution containing 10^{-4} M DNA and 10^{-5} M EB ([DNA]/[EB] = 10:1) was prepared for EB-DNA competitive binding studies. The quenching constants of the test compounds were calculated according to the classic Stern–Volmer equation: $I_0/I = 1 + K_q \times [Q]$,[39] where I_0 and I are the peak emission intensity of the EB-DNA system in the absence and presence of the quencher, $[Q]$ is the concentration of each quencher compound, and K_q is the Stern–Volmer quenching constant, which is obtained by the linear fit of plotting I_0/I versus $[Q]$ and determines the efficiency of the quencher. All the spectroscopic experiments were kept at 25 °C. In DNA viscosity measurements, ct-DNA is dissolved in BPE buffer (6 mM Na_2HPO_4, 2 mM NaH_2PO_4, 1 mM Na_2EDTA, pH = 7.2) to prepare 1×10^{-3} M working solution. Compounds were added with increasing concentrations from 2×10^{-5} M to 2×10^{-4} M to reach the [compound]/[DNA] ratios range from 0.02 to 0.20. Circulating bath temperature was maintained at 35.0 ± 0.1 °C. Viscosity values, η, (unit: cP) were directly obtained by running 0# spindle in working samples at 30 rpm. Data were presented as η/η_0 versus [compound]/[DNA] ratio, in which η_0 and η refers to viscosity of each DNA working sample in the absence and presence of added compound. Influence of DMSO as solvent on viscosity was eliminated based on its viscosity value of 2.03 cP measured at 35.0 °C.

Agarose Gel Electrophoresis Assay.[40] In plasmid DNA unwinding experiments, all compounds were prepared as 2×10^{-3} M stock solutions of DMSO and diluted to 10 and 100 μM by 1× TBE buffer. Compounds of various concentrations were mixed with 0.5 μg DNA and made up to a total 25 μL by TBE buffer so that the same experiment can be repeated twice. All samples were incubated at 25 °C in dark for 4 h. Then 12 μL of each sample mixed with 2 μL DNA loading buffer was electrophoresed at 5 V/cm through 0.8% agarose gel immersed in 1× TBE buffer solution for 60 min. Finally, the gel was stained with EB (1.27 μM) in dark for 30 min, followed by visualized on a BIO-RAD imaging system with a UV–vis trans-illuminator.

RESULTS AND DISCUSSION

Synthesis and Characterization of Oxoglaucine. On the basis of the relate references,[41,42] oxoglaucine was synthesized from (+)-boldine in two steps (Scheme 1). A facile large-scale semisynthesis of (+)-glaucine (1,2,9,10-tetramethoxyaporphine) from the commercially available (+)-boldine (2,9-dihydroxy-1,10-dimethoxyaporphine) by treatment of (+)-boldine with the conventional O-methylation reagents for the phenolic group such as PhN + $(CH_3)_3Cl^-$ under basic conditions afforded quaternary ammonium salt predominantly for (+)-boldine being a tertiary amine. But the raw product is a mixture and need to be purified on a silica gel column four times, the yield is lower than that of reference.[43] The (+)-glaucine product was confirmed by elemental analysis, APCI-MS, ^{1}H NMR, and ^{13}C NMR spectroscopy, which agree well with the reference values.[44,45]

On the basis of the reported method by Lee et al., (+)-glaucine was oxidized with manganese(III) acetate (MTA) under mild conditions to give oxoglaucine, but our yield was lower than that reported. The identity of the oxoglaucine was confirmed by elemental analysis, APCI-MS, ^{1}H NMR, and ^{13}C NMR. In particular, we for the first time report

dx.doi.org/10.1021/ic200443p | Inorg. Chem. 2012, 51, 1998–2009

the crystal structure of oxoglaucine. The crystal data and refinement details of oxoglaucine are summarized in Table 1, and the important bond lengths and angles are listed in the caption of Figure 2. As shown in Figure 2, similar to

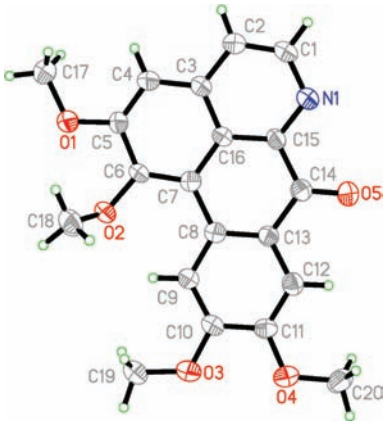

Figure 2. ORTEP view of oxoglaucine showing atom labeling, thermal ellipsoids are drawn at the 30% probability. Selected bond distances (Å) and angles (deg): C(1)−N(1) 1.338(5), C(15)−N(1) 1.328(4), C(14)−O(5) 1.367(4), C(5)−O(1) 1.367(4), C(6)−O(2) 1.373(4), C(10)−O(3) 1.365(4), C(11)−O(4) 1.364(4); N(1)−C(15)−C(14) 115.3(3), C(15)−C(14)−O(5) 121.1(4), C(5)−O(1)−C(17) 116.5(3), C(6)−O(2)−C(18) 115.8(3), C(10)−O(3)−C(19) 118.0(3), C(11)−O(4)−C(20) 117.4(3).

liriodenine,[12] oxoglaucine is a planar molecule with N(1) and carbonyl O(5) as potential donors. The structure of oxoglaucine is comparable with *O*-acetylisomoschatoline[46] and oxocrebanine.[47] In oxoglaucine, the four fused rings are essentially coplanar, while the four −OMe groups not coplanar with the ring system.

Characterization of Metal Complexes. Analytical data are in agreement with their formulations. The ^{1}H and ^{13}C NMR spectral data of complexes **1** and **2** along with their assignments are given in the Experimental Section. From the elemental analysis results, the desired metal complexes of OG were of sufficient purity.

Formation of metal complexes was confirmed by ESI mass spectrometry (see Supporting Information, Figure S3), capillary electrophoresis as well as fluorescence polarization. The spectra of complex **1** in DMSO−methanol showed peaks with m/z 338.84 (negative) and 352.12 (positive), which were attributed to $[AuCl_4]^-$ and $[OGH]^+$. The spectra of complexes **2**−**4** in DMSO−methanol showed peaks with m/z 828.14 (**2**), 860.10 (**3**), 856.11 (**4**) were assigned to $[Zn(OG)_2{+}NO_3]^+$, $[Co(OG)_2{+}ClO_4]^+$, $[Mn(OG)_2{+}ClO_4]^+$, respectively. In addition peaks with m/z 383.07 (**2**), 380.58 (**3**), 378.58 (**4**), which were attributed to $[Zn(OG)_2]^{2+}$, $[Co(OG)_2]^{2+}$, and $[Mn(OG)_2]^{2+}$, respectively, indicating that two aqua ligands easily disassociated. In some cases, peaks with medium m/z values of 558.63 (**1**), 556.13 (**2**), and 554.13 (**3**) were attributed to the formation of $[Zn(OG)_3]^{2+}$, $[Co(OG)_3]^{2+}$, and $[Mn(OG)_3]^{2+}$ in the mass spectrometer, similar to copper(II) complexes with modified indolo[3,2-*c*]quinoline ligands.[37] The observed isotopic patterns fit well with the theoretical isotopic distributions.

Due to complexes **2**−**4** having similar structures (inner-spheres), to confirm the formation of complexes, we selected complex **2** as representative to measure its capillary electrophoresis and fluorescence polarization. The capillary electrophoresis results of **2** and **OG** in DSMO−methanol−H_2O are shown in Figure S4 (see Supporting Information), which indicate that **2** differs strongly from that of OG; moreover **2** displays a strong single peak which confirms the formation zinc(II) complex.[48] In addition, since the fluorescence polarization P value is relevant to the bulk of fluorescent molecule. The P enhances with the bulk of fluorescent molecule increasing. Therefore the polarization value is expected to enhance after OG ligated to metal ion to form complex. Fluorescence polarization P values were determined in DMSO−methanol (v/v = 1:1) at 298 K exemplarity for complex **2** and OG using fluorescence polarization assay[49] ($\lambda_{max(ex)}$ = 379 nm, $\lambda_{max(em)}$ = 570 nm) under the same molar concentrations and experimental conditions. Comparison of P_{OG} (0.148) and $P_{complex2}$ (0.171) reveals that the P value of complex **2** significantly enhanced, which further confirms the formation of zinc(II) complex and is agreement with their results of ESI-MS and capillary electrophoresis.

Crystal Structures of Complexes 1−4. The molecular structures of gold(III) complex **1** is shown in Figure 3. Selected

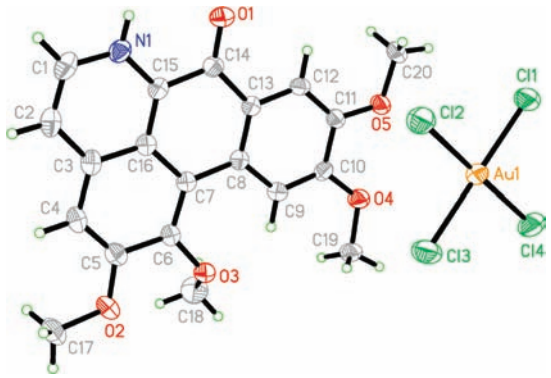

Figure 3. ORTEP view of [OGH][$AuCl_4$]·DMSO (**1**) showing atom labeling. Thermal ellipsoids are drawn at the 30% probability, and DMSO solvent molecules have been omitted for clarity. Selected bond distances (Å) and angles (°): C(1)−N(1) 1.344(6), C(15)−N(1) 1.338(5), C(14)−O(1) 1.225(5), Au(1)−Cl(1) 2.2695(13), Au(1)−Cl(2) 2.2735(14), Au(1)−Cl(3) 2.2753(14), Au(1)−Cl(4) 2.2760(13); N(1)−C(15)−C(14) 116.2(4), C(15)−C(14)−O(1) 121.1(4), C(5)−O(1)−C(17) 119.1(4), Cl(1)−Au(1)−Cl(2) 90.30(5), Cl(1)−Au(1)−Cl(3) 179.53(5), Cl(2)−Au(1)−Cl(4) 178.02(6).

bond distances (Å) and bond angles (deg) are given in the legend to the figure. Complex **1** crystallized in the monoclinic space group $P2(1)/n$. **1** is an ionic compound and comprises one oxoglaucine cation, one $[AuCl_4]^-$ anion, and one DMSO solvent. In **1**, oxoglaucine (OG) is protonated at N(1) to form a cation and does not contact Au(III) directly, and gold(III) tetrachloride serves as the counterion. The $[AuCl_4]^-$ anion has the square planar structure commonly observed for gold(III).[50] The Au−Cl bond lengths in the anion (2.2719−2.2760 Å) are very similar to those previously reported for other chlorogold(III) complexes.[51] The geometric parameters of oxoglaucine cation are comparable to those of oxoglaucine, and oxoglaucine still retains its planar structure, which can intercalate between the neighboring base pairs of DNA. But **1** is not a metallointercalator since Au is not involved in the intercalation.

The results of X-ray diffraction studies of complexes **2**−**4** are shown in Figure 4 (for complexes **3** and **4** see Supporting

dx.doi.org/10.1021/ic200443p | *Inorg. Chem.* 2012, 51, 1998−2009

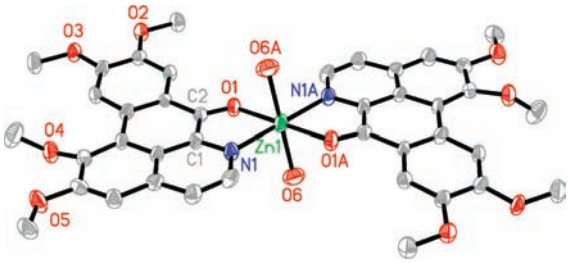

Figure 4. ORTEP view of $[Zn(OG)_2(H_2O)_2](NO_3)_2$ (**2**) showing atom labeling. Thermal ellipsoids are drawn at the 30% probability, and hydrogen atoms, as well as two NO_3^- or ClO_4^- anions, have been omitted for clarity. Selected bond distances (Å) and angles (deg) in **2**: Zn(1)−N(1) 2.079(5), Zn(1)−O(1) 2.103(6), Zn(1)−O(6) 1.367(4), N(1)−Zn(1)−O(1) 78.68(18), N(1)−Zn(1)−O(6) 90.7(2), O(1)−Zn(1)−O(6) 95.1(2), O(6)−Zn(1)−O(6A) 180.000(1), N(1)−Zn(1)−O(1A) 101.32(18), N(1)−Zn(1)−N(1A) 180.000(1) (A: $-x + 2, -y + 1, -z + 1$).

Information, Figures S5, S6), and selected bond lengths and bond angles are given in the caption. Three complexes crystallized in the triclinic space group $P\bar{1}$. Since complexes **2**−**4** possess general formula $[M(OG)_2(H_2O)_2](NO_3/ClO_4)_2$ (M = Zn, Co, Mn) and similar structure (inner-sphere), except for their different metal center and outer-sphere anion, therefore, herein only the structure of **2** is discussed. As shown in Figure 4, in one symmetry unit, **2** consists of one complex cation $[Zn(OG)_2(H_2O)_2]^{2+}$ and two NO_3^- anions. The zinc ion exhibits a distorted octahedral environment surrounded by the two N and two O atoms from the two bidentate oxoglaucine (OG) ligands and the two O atoms of the aqua ligands in trans position. Atoms O(1), N(1), O(1A), and N(1A) constitute the equatorial plane of the octahedron. Such structural characteristics was also observed in the liriodenine−cobalt(II) complex,[12] which retains an approximate planarity and can behave like a metallointercalator to intercalate between the neighboring base pairs of DNA to give high cytotoxicity.

In Vitro Cytotoxicity Assay. The in vitro cytotoxicity of oxoglaucine and its gold(III), zinc(II), cobalt(II), and manganese(II) complexes **1**−**4** were evaluated by the MTT method against five typical human tumor cell lines (using cisplatin as the positive control) involving liver, gastric adenocarcinoma, cervix, breast adenocarcinoma, and lung cancers. As shown in Table S1 (see Supporting Information), after the tumor cells were incubated with 20 μM test compounds for 48 h, each compound exhibited different antitumor activity. The inhibition rates of 20 μM OG ranged in 8%−15% toward all selected cells except HeLa, for which OG showed no inhibitory effect. In contrast to the free OG, the OG−metal complexes **1**−**4** generally exhibited significantly enhanced cytotoxicity. The inhibitory rates of **1** toward BEL7404, SGC 7901, MCF-7, and A549 were 82.91 ± 1.36, 45.15 ± 3.55, 31.05 ± 2.50, and 73.50 ± 0.70%, respectively. The inhibitory rates of **2** and **3** against HeLa were 53.85 ± 3.61 and 60.08 ± 3.14%, respectively; and that of **4** against SGC 7901 was 54.57 ± 1.54%. From Table S2 (see Supporting Information), it was found that without the OG ligand, none of the metal salts could exhibit an inhibition rate of >56% toward the five tested tumor cell lines even at 100 μM concentration of the metal salts. These results clearly suggested that the metal salts alone did not play a key role in the antitumor function, and the combination of OG with the metal produced appreciable synergetic effect. The IC_{50} values in Table 2 further showed various cytotoxicity of these OG-metal complexes. The IC_{50} value (6.1 μM) of **1** toward BEL7404 was lower than that of the divalent late transition metal complexes of liriodenine (IC_{50}= 8.4−112.1 μM)[12b] and $[Cu(PLN)(bipy)(H_2O)]_2(NO_3)_2{\cdot}4H_2O$ (IC_{50} = 12.9 μM, PLN = plumbagin, bipy =2,2′-bipyridine),[12c] as well as cisplatin. The activity of **2** and **3** (IC_{50} = 16.4 and 11.4 μM) against HeLa was lower than that of cisplatin, but is higher than that of the divalent late transition metal complexes of liriodenine (IC_{50}= 6.4−9.8 μM).[12b] In addition, **3** and **4** (IC_{50} = 5.1 and 7.8 μM) were more active toward MCF-7 than OG does (IC_{50} = 11.1 μM) and similar to cisplatin, and **1** (IC_{50} = 1.4 μM) exhibits higher activity toward A549 than free ligand OG and cisplatin. To sum up, these OG-metal complexes have different activity profile against the tested cell lines even though complexes **2**−**4** possess similar structure (inner-sphere). Such phenomenon is difficult to explain. In fact, except for cisplatin, there is relatively little mechanistic information on how metal anticancer drugs function, but it is clear that different metal ions can work through different routes that lead to different cellular responses.[52]

DNA Binding Studies. Despite the presence of other biological targets in tumor cells, including RNA, enzyme, and protein, it is generally accepted that DNA is the primary target for many metal-based anticancer drugs such as cisplatin.[53] Here we only consider DNA as the main target in the cell and leave the possible interaction of the OG−metal complexes with other targets, such as RNA, enzyme, and protein for future studies. The interactions between small molecules and DNA are known to be the primary action mechanisms of antitumor activity. In general, the interactions between small molecules and DNA include covalent binding and noncovalent binding, and the noncovalent bindings include intercalation, insertion, groove binding, electrostatic interaction, etc.[30b,54] The typical oxoaporphine alkaloids have been proven to realize antitumor activity by intercalating the neighboring base pairs of DNA to block DNA replication.[55] Our previous work indicated that the

Table 2. IC_{50} Values (μM)[a] for Compounds 1−4 and Cisplatin in Panel of Five Human Cancer Cell Lines

	BEL7404	SGC7901	HeLa	MCF-7	A549
OG	>150	>150	>150	11.1 ± 0.6	>150
1	6.1 ± 0.5	>150	>150	>150	1.4 ± 0.7
2	>150	>150	16.4 ± 4.5	>150	>150
3	13.1 ± 8.1	32.7 ± 0.8	11.4 ± 5.0	5.1 ± 0.8	>150
4	>150	No data	>150	7.8 ± 1.0	>150
cisplatin	132.8 ± 1.2	>150	>150	8.3 ± 1.0	25.3 ± 3.1

[a]IC_{50} values are presented as the mean ± SD (standard error of the mean) from five separated experiments. Cisplatin was used as a reference metallodrug and DMSO was used as a solvent control.

dx.doi.org/10.1021/ic200443p | Inorg. Chem. 2012, 51, 1998−2009

metal complexes of liriodenine, which is also an oxoaporphine alkaloid, might act as bifunctional DNA-binding compounds in which the liriodenine ligand intercalates between the neighboring base pairs of DNA and the metal cations such as platinum(II) and zinc(II) covalently bind to DNA. To investigate the DNA binding properties of oxoglaucine and its metal complexes, a series of spectroscopic studies were carried out, including UV−vis, fluorescence, CD spectra, viscosity measurements, and agarose gel electrophoresis assay. Because **3** and **4** are iso-structures, complex **4** was evaluated only by CD spectra.

UV−vis Spectral Analysis. It is well documented that intercalative $\pi-\pi$ stacking of the aromatic rings in the metal complexes with the DNA bases affects the transition dipoles of the molecules and usually leads to a reduction in their absorbance.[56] The UV−vis absorption was primarily used to discuss the binding mode of **2** to ct-DNA.

The UV−vis absorption spectra of **2** in the absence and presence of calf thymus DNA (ct-DNA) are shown in Figure 6

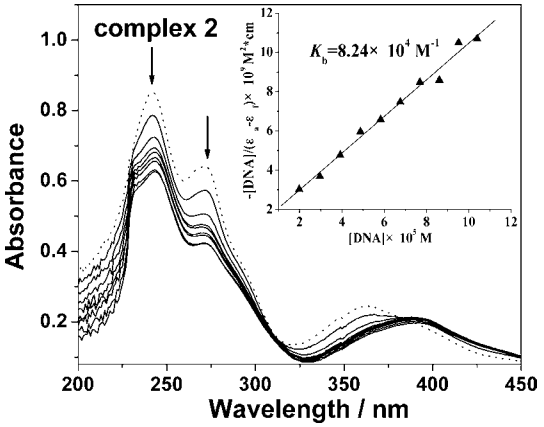

Figure 6. UV−vis absorption spectra of **2** in the absence (···) and presence (—) of ct-DNA with increasing [DNA]/[**1**] ratios range from 0.5:1 to 6:1.

(for OG, **1** and **3** see Supporting Information, Figure S7). In the absence of DNA, complexes **2**, **3**, and the free OG all showed characteristic absorption peaks at ∼245 and 272 nm (for complex **1**, absorption peaks were shown at 253 and 307 nm), which is ascribed to the $\pi \rightarrow \pi^*$ electronic transition of the conjugated system of oxoglaucine. Considering the absorption influence of DMSO at ∼250−260 nm, the absorbance at 272 nm for OG, complexes **2**, **3** and 307 nm for complex **1** was analyzed upon addition of ct-DNA. When the ratio of [DNA]/[OG] was increased from 0.5:1 to 6:1, a moderate hypochromicity of 17.6% and a slight red-shift were observed, suggesting the characteristic intercalation of OG to DNA with a moderate degree of binding. The steric hindrance of the four methoxyl groups in OG may have prevented more effective intercalation. Under similar conditions, evident hypochromicity for **1**−**3** (18.7% for **1**, 34.0% for **2**, 46.5% for **3**) were also observed along with the corresponding red-shifts. Especially, the 46.5% hypochromicity of **3** was obtained only at a relatively lower [DNA]/[**3**] ratio of 4:1. For further quantitative comparison, the intrinsic binding constant K_b was also calculated. The K_b values for OG and complexes **1**−**3** are 2.71×10^3, 1.62×10^4, 8.24×10^4, and 5.82×10^4 M^{-1}, respectively (inset plot of Figure 6; for OG, **1** and **3** see Supporting Information, inset plot of Figure S7), suggesting that complexes **1**, **2**, and **3** have stronger intercalative binding ability to DNA than OG.[55] According to their crystal structures, **1** is not a metallointercalator, whereas **2** and **3** are metallointercalators that have reinforced binding ability to DNA. However, because of the different nature of the metals, the binding abilities of **2** and **3** to DNA are different.

Competitive Binding Studies by Fluorescence Spectra. The binding abilities of OG and complexes **1**−**3** to ct-DNA were further investigated by competing with ethidium bromide (EB) as an intercalative probe.[57] In the competitive binding experiments, the EB-DNA system with [EB]/[DNA] = 1:10 ([EB] = 1×10^{-5} M, [DNA] = 1×10^{-4} M) showed the characteristic strong emission at ∼588 nm when excited by 332 nm light, indicating that the intercalated EB molecules had been sufficiently protected by the neighboring base pairs in the DNA from being quenched by polar solvent molecules. When increasing the concentration of **2** from [**2**]/[EB] = 1:1 to 4:1, the characteristic emission of EB was decreased significantly, as shown in Figure 7 (for OG, **1** and **3** see Supporting

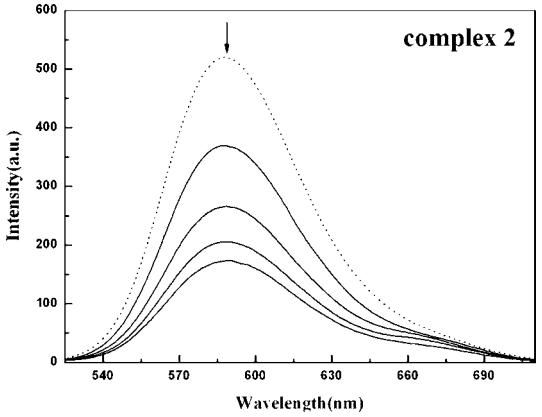

Figure 7. Fluorescence emission spectra of EB bound with ct-DNA in the absence (dashed line ----) and presence (solid lines —) of **2** as competitive agent with increasing [**2**]/[EB] ratios of 1:1 to 4:1.

Table 3. Calculated Quenching Ratios of EB by Titration of OG/Complexes to EB-ctDNA System

compound	one-step FI quenching ratio (%)[a]	total FI quenching ratio	K_q
OG	13.9	54.7% at [OG]/[EB] = 6:1	7.1×10^3
1	18.1	69.0% at [**1**]/[EB] = 9:1	1.3×10^4
2	29.1	78.1% at [**2**]/[EB] = 4:1	2.7×10^4
3	28.0	71.6% at [**3**]/[EB] = 6:1	2.2×10^4

[a]FI, fluorescence intensity; one-step refers to [compound]/[EB] = 1:1.

Information Figure S8). Table 3 lists the corresponding quenching data of EB fluorescence intensity and the calculated competitive binding ability. It was found that the metal complexes and OG could all effectively quench the fluorescence emission of EB, which strongly suggests that they may compete with EB to bind to DNA through intercalation at the similar binding site.[58]

dx.doi.org/10.1021/ic200443p | Inorg. Chem. 2012, 51, 1998−2009

Furthermore, the quenching constants K_q were also calculated by restricted linear fitting of $[I_0/I]$ to $[Q]$ from the Stern–Volmer equation and listed in Table 3. The calculated K_q for OG is 7.1×10^3, while those for complexes **1**, **2**, **3** are 1.3×10^4, 2.7×10^4, and 2.2×10^4, respectively. All the three complexes exhibited stronger quenching ability than OG, which is consistent with the UV–vis spectral titration results. It seems that combining OG with the metal ions will reinforce its binding to ct-DNA and the metal ions play important roles in the high cytotoxicity of the OG-metal complexes. Even though the binding of these complexes can only induce small structural changes in the DNA duplex, they lead to a different cellular response.[59]

Circular Dichroism Spectral Analysis. Circular dichroism (CD) is a useful technique to assess whether nucleic acids undergo conformational changes as a result of complex formation or changes in environment.[60] The normal ct-DNA has a right-handed chiral conformation and exists in B-form in solution. The CD spectrum of DNA is very sensitive to its conformational changes. It is generally accepted that covalent binding and intercalative binding can influence the tertiary structure of DNA and induce changes in the CD spectra of DNA, whereas other noncovalent binding modes such as electrostatic interaction or groove binding cannot significantly perturb the CD spectra.[61]

The CD absorption of ct-DNA shows a positive absorbance peak at ~270 nm and a negative absorbance peak at *ca.* 245 nm (shown as dashed line in CD spectra), due to the $\pi-\pi$ base stacking of DNA and the right-hand helicity of B-form DNA, respectively.[62] The addition of OG did not perturb the CD spectrum of DNA until [OG] reached 5×10^{-5} M, when both the positive and the negative absorbance of DNA evidently decreased (for OG, **1**, **3**, and **4**, see Supporting Information, Figure S9). Intercalation is the most probable binding mode between OG and DNA because of the planar aromatic structure of OG, but the intercalative ability of OG to DNA appears weak. However, the addition of complex **2** induced significant changes in the characteristic absorption of DNA, which indicates the formation of a steady complex between DNA and **2**, as shown in Figure 8.[63] At lower concentrations of **2** (5

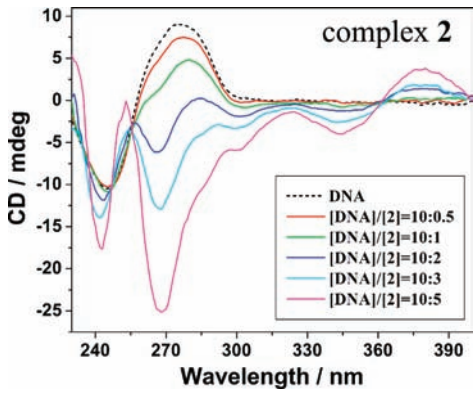

Figure 8. Circular dichroism spectra of ct-DNA bound by **2** with [DNA]/[**2**] ratios range from 10:0.5 to 10:5 (DNA alone of 1×10^{-4} M, dashed line; DNA bound by **2** with increasing concentrations, colored solid lines).

$\times 10^{-6}$ M and 1×10^{-5} M), there was significant decrease in the positive absorbance (with 18.4%–53.6% hypochromicity and 3–5 nm bathochromic shift, respectively) but no change in the negative absorption in the CD spectra, which represents the intercalative binding of **2** to DNA. At higher concentrations of **2** (from 2×10^{-5} M to 5×10^{-5} M), there were dramatic changes in the CD absorption of DNA and the characteristic DNA absorption peaks disappeared, which indicates the transformation from B-form to non-B-form DNA secondary structure.[64] Furthermore, induced positive and negative CD signals respectively at ~380 and 345 nm could be observed in the CD spectrum, which resulted from the binding of complex **2** to DNA as a metallointercalator.[65]

The changes in the CD spectra of the DNA upon addition of complex **4** are very similar to those of complex **2** (see Supporting Information, Figure S9), which strongly suggests that **4** and **2** have the same binding mode toward ct-DNA, especially considering their similar structure and coordination mode. Because complex **3** has poor solubility in water and precipitates at higher concentration, only two CD spectra of DNA binding with **3** were scanned at [DNA]/[**3**] molar ratios of 10:0.5 and 10:1 respectively. Nevertheless, the significant decreases in the positive absorbance and the slight decreases in the negative absorbance, along with the unchanged CD absorption curves, also suggests the intercalative binding of **3** at low concentration ($\leq 1 \times 10^{-5}$ M) toward ct-DNA.[66] Under the same conditions, complex **1** did not induce such dramatic changes in the CD spectrum of DNA as complexes **2**–**4** did, which should be due to the different structure of **1** to those of **2**–**4**. Similar to OG, complex **1** also induced slight but regular decreases in the positive absorption without changing the negative absorption at lower concentration, and induced more significant decreases in both the positive and the negative absorption at higher concentration, which evidently indicates a weak intercalative binding of **1** to DNA without DNA cleavage.[67]

DNA Viscosity Experiments. It is generally accepted that besides X-ray crystallography and high-resolution NMR, the viscosity measurement of DNA solution can also serve as a quite unambiguous method to distinguish the binding modes of small molecules to DNA. When small planar aromatic molecules intercalate between the neighboring base pairs of DNA, the double helix loosens to accommodate the intercalation, which increases the length of the DNA helix. Since the viscosity of DNA solution is very sensitive to the changes of DNA length, the increased viscosity of DNA solution can be associated with the specific intercalation binding mode.[68]

The viscosity of the ct-DNA solution increased notably after the addition of OG, OG-metal complex or EtBr, as shown in Figure 9. When increasing the [compound]/[DNA] ratios from 0.02 to 0.20, the viscosity of the DNA solution bound with OG or its three complexes **1**–**3** all increased regularly. Complexes **2** and **3** exhibited similar behavior and both increased the viscosity slightly more than OG did when the [compound]/[DNA] ratio was in the range of 0.02–0.16. Despite the apparent differences in the strength of interaction, OG, **2**, and **3** all exhibited similar viscosity enhancement profile compared with EtBr, which clearly suggests that intercalation is the main binding mode for their interaction with ct-DNA. In contrast to **2** and **3**, **1** increased the viscosity of DNA solution much less effectively, which suggests that other binding modes, such as electrostatic interaction may exist between **1** and DNA and play important role.[69]

In summary, the UV–vis spectral titration revealed that the binding of **1**–**3** to ct-DNA was mainly through the intercalation

dx.doi.org/10.1021/ic200443p | *Inorg. Chem.* 2012, 51, 1998–2009

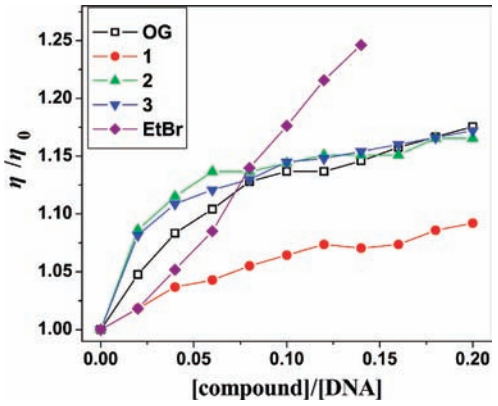

Figure 9. Relative viscosity increments of ct-DNA solution bound with **OG**, complexes **1**−**3**, and EtBr with increasing [compound]/[DNA] ratios range from 0.02 to 0.20 every 0.02 interval.

of complexes **1**−**3**. The OG metal complexes have stronger binding ability than OG. Furthermore, the EB-competitive binding studies indicated that complexes **1**−**3** had higher competitive binding ability than OG against EB in the ct-DNA system. The complexes **2**−**4** induced significant perturbation in the CD spectra of ct-DNA but complex **1** did not, and complexes **2** and **3** could increase the viscosity of DNA solution much more effectively than **1**. Thus it can be seen that the OG-metal complexes bind to DNA more strongly than OG. These findings agree well with the fact that the cytotoxicity of complexes **1**−**4** toward most tested tumor cell lines are higher than that of OG alone because the planar OG ligand in complexes **1**−**4** can bind more powerfully to DNA than the free OG and the metal ions also play key roles in their cytotoxicity.

Agarose Gel Electrophoresis Assay. The binding modes of OG and complexes **1**−**3** to pUC19 plasmid DNA were further examined by agarose gel electrophoresis assay. As shown in Figure 10, upon addition of OG and increasing its

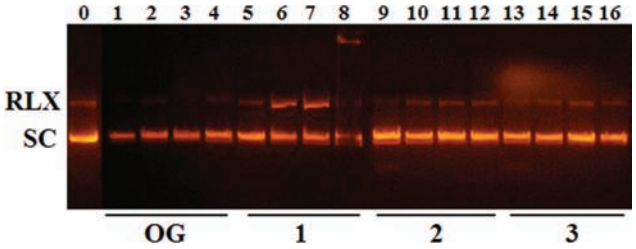

Figure 10. Agarose gel electrophoresis of pUC19 DNA treated with OG and complexes **1**−**3** after incubation for 1 h at 37 °C. Lane 0: DNA alone. Lanes 1−4, 5−8, 9−12 and 13−16 refer to DNA in the presence of OG and complexes **1**−**3**, respectively, at 10, 25, 50, and 100 μM; SC, supercoiled form, RLX, relaxed form.

concentration from 10 to 100 μM in the absence of any external reagent or light, the DNA decreased significantly in both the major supercoiled form and the minor relaxed form. The addition of **2** and **3** did not significantly change the DNA either in the supercoiled or the relaxed form, as shown by the migration rate and proportions. Therefore, **2** and **3** have weak unwinding ability for supercoiled DNA. But in the presence of **1** at 25 and 50 μM, more DNA in the relaxed form can be clearly observed, which suggests that **1** has different binding modes compared with other complexes and is consistent with the results from the spectral analyses and DNA viscosity experiment.

Topoisomerase I Inhibition Studies. Topoisomerases are ubiquitous molecules that relieve the torsional stress in the DNA helix generated as a result of replication, transcription, and other nuclear processes. They are also the specific targets of a number of anticancer agents, including camptothecins, indolocarbazoles, indenoisoquinolines, etoposide, and adriamycin. These anticancer agents bind to a transient topoisomerase I (TOPO I)-DNA covalent complex and inhibit the resealing of a single-strand nick that the enzyme creates to relieve the superhelical tension in duplex DNA.[70]

The TOPO I inhibition ability of OG and complexes **1**−**3** is shown in Figure 11. Lanes 1 and 2 show the unwinding of

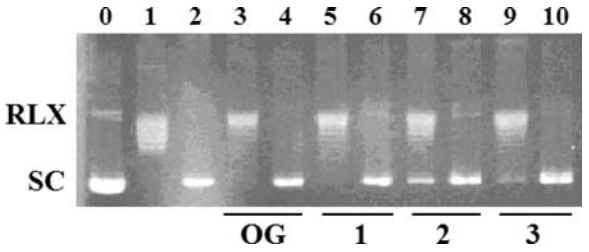

Figure 11. Inhibition of TOPO I-mediated DNA relaxation by OG and complexes **1**−**3**, respectively. Lane 0: DNA alone. Lane 1: DNA + TOPO I. Lane 2: DNA + TOPO I + HCPT (50 μM). Lanes 3−4, 5−6, 7−8 and 9−10 refer to DNA + TOPO I + OG/complexes **1**−**3** at 50, 100 μM, respectively.

supercoiled DNA by TOPO I and the inhibition ability of camptothecin as a classic TOPO I inhibitor. The presence of OG or **1**−**3** at 50 μM did not show obvious inhibition of TOPO I, but at a higher concentration of 100 μM, they all effectively inhibited TOPO I from unwinding supercoiled DNA. The observed results suggest that the TOPO I inhibition ability of these complexes should originate from the OG moiety.

S-Phase Cell-Cycle Arrest. To determine whether cellular DNA is a major target of the OG-metal complexes, we studied the cell-cycle profiles of cancer cells treated with **1**−**3**. Cell-cycle analysis was performed by using flow cytometry to assess the DNA content of cells, which was stained with propidium iodine (PI). This enables the quantification of the total cellular populations in different phases of the cell cycle (G0/G1, S, and G2/M). The flow cytometric data for BEL7404 cells treated with **1**−**3** are shown in Figure 12. Treatment of cells with **1**−**3** (10 μM) for 24 h enhanced cell-cycle arrest at the S phase, resulting in concomitant population increase in the S phase and population decrease in the G1 phase, the stage in which most DNA replication occurs.[71] The direct interaction of **1**−**3** with DNA has been examined. We found that compounds **1**−**3** strongly interact with ct-DNA with binding constants of 1.62×10^4, 8.24×10^4, and 5.82×10^4 M^{-1}, respectively, based on the results from spectrophotometric titration experiments. Complexes **1**−**3** are able to intercalate between the neighboring base pairs of DNA and have inhibitory activity on a DNA-binding protein topoisomerase I. Taking these results altogether, DNA may be a crucial cellular target for **1**−**3** to achieve cytotoxicity.

■ CONCLUSIONS

The TCM active component oxoglaucine was synthesized and reacted with Au(III), Zn(II), Co(II), and Mn(II) salts to give

dx.doi.org/10.1021/ic200443p | Inorg. Chem. 2012, 51, 1998−2009

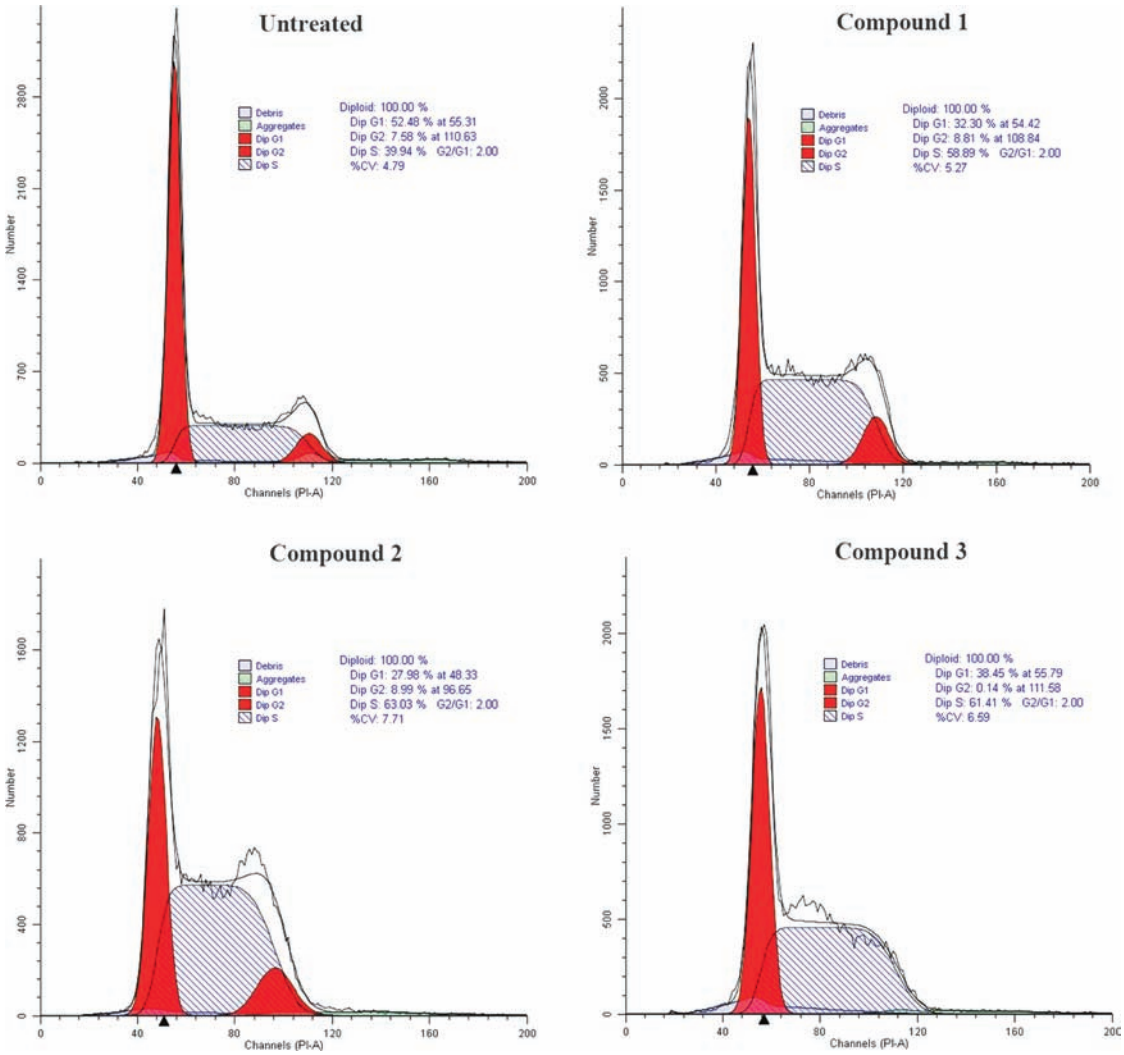

Figure 12. Induction of cell-cycle arrest in BEL7404 cells after treatment with **1**−**3**. Untreated cells and cells treated with **1**−**3** (10 μM) were collected at 24 h, subjected to PI staining and flow cytometric analysis. G0/G1, G2/M, and S indicate the cell phase. Data shown is a representative experiment repeated twice with similar results.

four oxoglaucine−metal complexes. The complexes were characterized and their crystal structures were determined by X-ray diffraction. The oxoglaucine−Au(III) compound **1** was ionic and the Au metal was not directly bonded to oxoglaucine. The other complexes **2**−**4** were coordination compounds with chelated bonding between oxoglaucine and the metal, which were further confirmed by ESI-MS, capillary electrophoresis and fluorescence polarization; even though they might dissociate and release positively charged species in solution. The in vitro cytotoxicity of **1**−**4** against five selected human tumor cell lines is different. In some cases, they exhibited significant enhanced antitumor activity compared with those of oxoglaucine and corresponding metal salts, such as **1** toward BEL7404 and A549; **2** and **3** toward HeLa, **3** and **4** toward MCF-7. It seems that these OG-metal complexes were selectively active against certain cell lines. Although the spectroscopic and agarose gel electrophoresis results showed that the binding of these compounds to DNA could only induce small structural changes in the duplex, it could lead to a different cellular response.[59] The cell cycle analyses showed that **1**−**3** increased cell cycle arrest at the S phase. These OG−metal compounds interacted with ct-DNA mainly through intercalation and could effectively inhibit TOPO I, implying that topoisomerase I may be yet another molecular target. However, the exact molecular mechanism requires further detailed investigation.

■ ASSOCIATED CONTENT

Ⓢ Supporting Information

Further details are given in Figures S1−S9, Tables S1 and S2, and X-ray crystallographic data is given in CIF format. These materials are available free of charge via the Internet at http://pubs.acs.org.

■ AUTHOR INFORMATION

Corresponding Author

*E-mail: chenzfubc@yahoo.com (Z.-F.C.); hliang@gxnu.edu.cn (H.L.). Tel.: +86(0)773/2120998. Fax: +86(0)773/2120958.

■ ACKNOWLEDGMENTS

This work was supported by National Basic Research Program of China (Nos. 2010CB534911, 2012CB723501), the National Natural Science Foundation of China (No. 20861002), and Natural Science Foundation of Guangxi Province (Nos.0991012Z, 0991003, and 2010GXNSFF013001), as well

as "BAGUI Scholar" program. We also thank Prof. Dr. Huai-Ming Hu for the crystal structures determination, Prof. Dr. Z. Guo from NJU and Prof. Dr. Chris Orvig from UBC for valuable discussion.

REFERENCES

(1) (a) Jung, Y.; Lippard, S. J. *Chem. Rev.* **2007**, *107*, 1387−1407. (b) Bruijnincx, P. C. A.; Sadler, P. J. *Curr. Opin. Chem. Biol.* **2008**, *12*, 197−206. (c) Hartinger, C. G.; Nazarov, A. A.; Ashraf, S. M.; Dyson, P. J.; Keppler, B. K. *Curr. Med. Chem.* **2008**, *15*, 2574−2591. (d) Kostova., I. *Curr. Med. Chem.* **2006**, *13*, 1085−1107. (e) Lovejoy, K. S.; Todd, R. C.; Zhang, S.; McCormick, M. S.; D'Aquino, J. A.; Reardon, J. T.; Sancar, A.; Giacomini, K. M.; Lippard, S. J. *Proc. Natl. Acad. Sci. U.S.A.* **2008**, *105*, 8902−8907.

(2) Jamieson, E. R.; Lippard, S. J. *Chem. Rev.* **1999**, *99*, 2467−2498.

(3) (a) Farrer, N. J.; Salassa, L.; Sadler, P. J. *Dalton Trans.* **2009**, 10690−10701. (b) Sun, R. W.-Y.; Ng, M. F.-Y.; Wong, E. L.-M.; Zhang, J.; Chui, S. S.-Y.; Shek, L.; Lau, T.-C.; Che, C.-M. *Dalton Trans.* **2009**, 10712−10716.

(4) Dyson, P. J.; Sava, G. *Dalton Trans.* **2006**, 1929−1933.

(5) Richardson, D. R.; Kalinowski, D. S.; Richardson, V.; Sharpe, P. C.; Lovejoy, D. B.; Isalam, M.; Bernhardt, P. V. *J. Med. Chem.* **2009**, *52*, 1459−1470.

(6) (a) Tiekink, E. R. T. *Inflammopharmacology* **2008**, *16*, 138−142. (b) Milacic, V.; Fregona, D.; Dou, Q. P. *Histol. Histopathol.* **2008**, *23*, 101−108. (c) Sun, R. W.-Y.; Che, C.-M. *Coord. Chem. Rev.* **2009**, *253*, 1682−1691. (d) Milacic, V.; Dou, Q. P. *Coord. Chem. Rev.* **2009**, *253*, 1649−1660. (e) Ott, I. *Coord. Chem. Rev.* **2009**, *253*, 1670−1681. (f) Bindoli, A.; Rigobello, M. P.; Scutari, G.; Gabbiani, C.; Casini, A.; Messori, L. *Coord. Chem. Rev.* **2009**, *253*, 1692−1707. (g) Fricker, S. P. *Metallomics* **2010**, *2*, 366−377.

(7) (a) Bench, B. A.; Beveridge, A.; Sharman, W. M.; Diebold, G. J.; van Lier, J. E.; Gorun, S. M. *Angew. Chem., Int. Ed.* **2002**, *41*, 748−750. (b) Xi, P.-X.; Xu, Z.-H.; Chen, Z.-Z.; Zhang, X.-W. *J. Inorg. Biochem.* **2009**, *103*, 210−218. (c) Tan, J.; Wang, B.; Zhu, L. *Bioorg. Med. Chem.* **2009**, *17*, 614−620. (d) Kowol, C. R.; Trondl, R.; Arion, V. B.; Jakupec, M. A.; Lichtscheidl, I.; Keppler, B. K. *Dalton Trans.* **2010**, 704−706. (e) Boerner, L. J. K.; Zaleski, J. M. *Curr. Opin. Chem. Biol.* **2005**, *9*, 135−144. (f) Franklin, R. B.; Costello, L. C. *Arch. Biochem. Biophys.* **2007**, *463*, 211−217.

(8) (a) Hambley, T. W. *Science* **2007**, *318*, 1392−1393. (b) Rubner, G.; Bensdrf, K.; Wellner, A.; Kircher, B.; Bergemann, S.; Ott, I.; Gust, R. *J. Med. Chem.* **2010**, *53*, 6889−6898. (c) Fail, T. W.; Culinane, C.; Diakos, C. I.; Yamamoto, N.; Lyons, J. G.; Hambley, T. W. *Chem.—Eur. J.* **2007**, *13*, 2974−2982. (d) Kamalakannan, P.; Venkappayya, D. *J. Inorg. Biochem.* **2002**, *90*, 22−37. (e) Afrasiabi, Z.; Sinn, E.; Padhye, S.; Dutta, S.; Padhye, S.; Newton, C.; Anson, C. E.; Powell, A. K. *J. Inorg. Biochem.* **2003**, *95*, 306−314. (f) Trávníček, Z.; KlanicováA.; Popa, I.; Rolčík. *J. Inorg. Biochem.* **2005**, *99*, 776−786. (g) Ware, D. C.; Brothers, P. J.; Clark, G. R.; Denny, W. A.; Palmer, B. D.; Wilson, W. R. *Dalton Trans.* **2000**, 925−932. (h) He, Z.; Lai, D.; Wakelin, L. P. G *Eur. J. Pharmacol.* **2010**, *637*, 11−15. (i) Bisceglie, F.; Baldini, M.; Belicchi-Ferrari, M.; Buluggiu, E.; Careri, M.; Pelosi, G.; Pinelli, S.; Tarasconi, P. *Eur. J. Med. Chem.* **2007**, *42*, 627−634. (j) Liang, F.; Wang, P.; Zhou, X.; Li, T.; Li, Z.; Lin, H.; Gao, D.; Zheng, C.; Wu, C. *Bioorg. Med. Chem. Lett.* **2004**, *14*, 1901−1904. (k) Milbank, J. B. J.; Stevenson, R. J.; Ware, D. C.; Chang, J. Y. C.; Tercel, M.; Ahn, G.-O.; Wilson, W. R.; Denny, W. A. *J. Med. Chem.* **2009**, *52*, 6822−6834.

(9) (a) Xu, Z.-D.; Liu, H.; Wang, M.; Xiao, S.-L.; Yang, M.; Bu, X.-H. *J. Inorg. Biochem.* **2002**, *92*, 149−155. (b) Xu, Z.-D.; Liu, H.; Xiao, S.-L.; Yang, M.; Bu, X.-H. *J. Inorg. Biochem.* **2002**, *90*, 79−84. (c) Chen, Q. Y.; Zhou, D.-F.; Huang, J.; Guo, W.-J.; Gao, J. *J. Inorg. Biochem.* **2010**, *104*, 1141−1147. (d) Alexandru, M.-G.; Velockovic, T. C.; Jitaru, I.; Grguric-Sipka, S.; Draghici, C. *Cent. Eur. J. Chem.* **2010**, *8*, 639−645.

(10) (a) To, K. K. W.; Au-Yeung, S. C. F.; Ho, Y.−P. *Anti-Cancer Drugs* **2006**, *17*, 673−683. (b) To, K. K. W.; Ho, Y.-P.; Au-Yeung, S. C. F. *Anti-Cancer Drugs* **2005**, *16*, 825−835. (c) Ho, Y.-P.; To, K. K. W.; Au-Yeung, S. C. F.; Wang, X.; Lin, G.; Han, X. *J. Med. Chem.* **2001**, *44*, 2065−2068.

(11) (a) Zinsmeister, H. D.; Becker, H.; Eicher, T. *Angew. Chem., Int. Ed.* **1991**, *30*, 130−147. (b) Wang, L.; Guo, S.; Chen, Y.; Liu, Y. *Bioorg. Med. Chem. Lett.* **2005**, *15*, 3417−3422. (c) Chen, Z.-F.; Liang, H. *Anti-Cancer Agents Med. Chem.* **2010**, *12*, 412−423.

(12) (a) Chen, Z.-F.; Liu, Y.-C.; Liu, L.-M.; Wang, H.-S.; Qin, S.-H.; Wang, B.-L.; Bian, H.-D.; Yang, B.; Fun, H.-K.; Liu, H.-G.; Liang, H.; Orvig, C. *Dalton Trans.* **2009**, 262−272. (b) Liu, Y.-C.; Chen, Z.-F.; Liu, L.-M.; Peng, Y.; Hong, X.; Yang, B.; Liu, H.-G.; Liang, H.; Orvig, C. *Dalton Trans.* **2009**, 10813−10823. (c) Chen, Z.-F.; Tan, M.-X.; Liu, L.-M.; Liu, Y.-C.; Wang, H.-S.; Yang, B.; Peng, Y.; Liu, H.-G.; Liang, H.; Orvig, C. *Dalton Trans.* **2009**, 10824−10833. (d) Chen, Z.-F.; Tan, M.-X.; Liu, Y.-C.; Peng, Y.; Wang, H.-H.; Liu, H.-G.; Liang, H. *J. Inorg. Biochem.* **2011**, *105*, 308−316. (e) Chen, Z.-F.; Mao, L.; Liu, L.-M.; Liu, Y.-C.; Peng, Y.; Hong, X.; Wang, H.-H.; Liu, H.-G.; Liang, H. *J. Inorg. Biochem.* **2011**, *105*, 171−180.

(13) Chang, F.-R.; Wei, J.-L.; Teng, C.-M.; Wu, Y.-C. *J. Nat. Prod.* **1998**, *61*, 1457−1461.

(14) Chen, Y. Y.; Chang, F.-R.; Wu, Y.-C. *J. Nat. Prod.* **1996**, *59*, 904−906.

(15) Chen, K.-S.; Chang, F.-R.; Chia, Y.-C.; Wu, T.-S.; Wu, Y.-C. *J. Chin. Chem. Soc.* **1998**, *45*, 103−110.

(16) Chen, C.-L.; Chang, H.-M.; Cowling, E. B.; Huang Hsu, C.-Y.; Gates, R. P. *Phytochemistry* **1976**, *15*, 1161−1167.

(17) Blanco, O. M.; Castedo, L.; Villaverde, M. C. *Phytochemistry* **1993**, *32*, 1055−1057.

(18) Tojo, E.; Dominguez, D.; Castedo, L. *Phytochemisrry* **1991**, *30*, 1005−1010.

(19) Ohiri, F. C.; Verpoorte, R.; Svendsen, A.; Baerheim, A. *Planta Med.* **1982**, *46*, 228−230.

(20) Orahovats, A. S.; Dutschewska, H. B.; Mollow, N. M. *Dokl. Bolg. Akad. Nauk* **1973**, *26*, 491−492.

(21) Sari, A. *Planta Med.* **1999**, *65*, 492.

(22) Wu, Z. Y.; Zhou, T. Y.; Xiao, P. G. *Xin Hua Compendium of Materia Medica (I)*; Shanghai Science & Technology Press: Sahnghai, 1998; pp 113−117.

(23) (a) Wu, Y.-C.; Liou, Y.-F.; Lu, S.-T.; Chen, C.-H.; Chang, J.-J.; Lee, K.-H. *Planta Med.* **1989**, *55*, 163−165. (b) Chen, S.-B.; Gao, G.-Y.; Yu, S.-C.; Xiao, P.-G. *Planta Med.* **2002**, *68*, 554−556. (c) Chang, F.-R.; Hsieh, T.-J.; Huang, T.-L.; Chen, C.-Y.; Kuo, R.-Y.; Chang, Y.-C.; Chiu, H.-F.; Wu, Y.-C. *J. Nat. Prod.* **2002**, *65*, 255−258.

(24) Jantan, I.; Raweh, S. M.; Yasin, Y. H. M.; Murad, S. *Phytother. Res.* **2006**, *20*, 493−496.

(25) (a) Ivanovska, N.; Philipov, S.; Georgieva, P. *Pharmacol. Res.* **1997**, *35*, 267−272. (b) Ivanovska, N.; Hristova, M.; Philipov, S. *Pharmacol. Res.* **2000**, *41*, 101−107.

(26) Ivanovska, N.; Hristova, M. *Diagn. Microbiol. Infect. Dis.* **2000**, *38*, 17−20.

(27) Remichkova, M.; Dimitrova, P.; Philipov, S.; Ivanovska, N. *Fitoterapia* **2009**, *80*, 411−414.

(28) Clark, A. M.; Watson, E. S.; Ashfaq, M. K.; Hufford, C. D. *Pharm. Res.* **1987**, *4*, 495−498.

(29) Jennette, K. W.; Lippard, S. J.; Vasiliades; Lippard, S. J. *Proc. Natl. Acad. Sci. U.S.A.* **1974**, *71*, 3839−3843.

(30) (a) Erkkilla, K. E.; Odom, D. T.; Barton, J. K. *Chem. Rev.* **1999**, *99*, 2777−2795. (b) Zeglis, B. M.; Pierre, V. C.; Barton, J. K. *Chem. Commun.* **2007**, 4565−4579.

(31) Liu, H.-K; Sadler, P. J. *Acc. Chem. Res.* **2011**, *44*, 349−359.

(32) Kumar, C. V.; Barton, J. K.; Turro, N. J. *J. Am. Chem. Soc.* **1985**, *107*, 5518−5523.

(33) Reichmann, M. F.; Rice, S. A.; Thomas, C. A.; Doty, P. *J. Am. Chem. Soc.* **1954**, *76*, 3047−3053.

(34) Sheldrick, G. M. *SADABS*, version 2.05; University of Göttingen: Göttingen, Germany, 2002.

(35) Sheldrick, G. M. *SHELXS-97, Program for Solution of Crystal Structures*; University of Göttingen: Göttingen, Germany, 1997.

(36) (a) Vekshin, N. L. *J. Biol. Phys.* **1999**, *25*, 339−354. (b) Yin, Y. -B.; Wang, Y. -N.; Ma, J. -B. *Spectrochim Acta A.* **2006**, *64*, 1032−1038.

(c) Yushchenko, D. A.; Vadzyuk, O. B.; Kosterin, S. O.; Duportail, G.; Mély, Y.; Pivovarenko, V. G. *Anal. Biochem.* **2007**, *369*, 218−225.
(37) Primik, M. F.; Göschl, S.; Jakupec, M. A.; Roller, A.; Keppler, B.; Arion, V. B. *Inorg. Chem.* **2010**, *49*, 11084−11095.
(38) Alley, M. C.; Scudiero, D. A.; Monks, A.; Hursey, M. L.; Czerwinski, M. J.; Fine, D. L.; Abbott, B. J.; Mayo, J. G.; Shoemaker, R. H.; Boyd, M. R. *Cancer Res.* **1988**, *48*, 589−601.
(39) (a) Stern, O.; Volmer, M. Z. *Z. Phys.* **1919**, *20*, 183. (b) Lakowicz, J. R.; Weber, G. *Biochemistry* **1973**, *12*, 4161−4170.
(40) Keck, M. V.; Lippard, S. J. *J. Am. Chem. Soc.* **1992**, *114*, 3386−3390.
(41) Huang, W.-J.; Chen, C.-S.; Singh, O. V.; Lee, S.-L.; Lee, S.-S. *Synth. Commun.* **2002**, *32*, 3681−3686.
(42) Singh, O. V.; Huang, W.-J.; Chen, C.-H.; Lee, S.-S. *Tetrahedron Lett.* **2007**, *48*, 8166−8169.
(43) Boente, J. M.; Castedo, L.; Cuadros, R.; de Lera, A. R.; Saá, J. M.; Suau, R.; Vidal, M. C. *J. Nat. Prod.* **1975**, *38*, 175−338.
(44) Boente, J. M.; Castedo, L.; Cuadros, R.; de Lear, A. R.; Saá, J. M.; Suau, R.; Vidal, M. C. *Tetrahedron Lett.* **1983**, *24*, 23030−2306.
(45) Marsaioli, A. J.; Magalhaes, A. F.; Ruveda, E. A.; Reis, F.; de, A. M. *Phytochemistry* **1980**, *19*, 995−997.
(46) Tavanaiepour, I.; Watson, W. H. *Acta Crystallogr., Sect. C: Cryst. Struct. Commun.* **1987**, *43*, 2230−2232.
(47) Din, L. B.; Zakaria, Z.; Abdullah, A.; Yamin, B. M. *Acta Crystallogr., Sect. E: Cryst. Struct. Rep. Online* **2005**, *61*, o1450−1452.
(48) Hartinger, C. G.; Keppler, B. K. *Electrophoresis* **2007**, *28*, 3436−3446.
(49) Ye, B.-C.; Yin, B.-C. *Angew. Chem., Int. Ed.* **2008**, *47*, 8386−8389.
(50) Johnson, S. W.; Shen, D.-W.; Pastan, I.; Gottesman, M. M.; Hamilton, T. C. *Exp. Cell Res.* **1996**, *226*, 133−139.
(51) Liu, H.; Zhao, F.; Yang, R.; Wang, M.; Zheng, M.; Zhao, Y.; Zhang, X.; Qiu, F.; Wang, H. *Phytochemistry* **2009**, *70*, 773−778.
(52) Vrzal, R.; Štarha, P.; Dvořák, Z.; Trávníček, Z. *J. Inorg. Biochem.* **2010**, *104*, 1130−1132.
(53) (a) Zhang, C. X.; Lippard, S. J. *Curr. Opin. Chem. Biol.* **2003**, *7*, 481−489. (b) Wu, C.-H.; Wu, D.-H.; Liu, X.; Guoyiqibayi, G.; Guo, D.-D.; Lv, G.; Wang, X.-M.; Yan, H.; Jiang, H.; Lu, Z.-H. *Inorg. Chem.* **2009**, *48*, 2352−2354.
(54) Maheswari, P. U.; Palaniandavar, M. *J. Inorg. Biochem.* **2004**, *98*, 219−230.
(55) (a) Galindo, M. A.; Olea, D.; Romero, M. A.; Gómez, J.; del Castillo, P.; Hannon, M. J.; Rodger, A.; Zamora, F.; Navarro, J. A. R. *Chem.—Eur. J.* **2007**, *13*, 5075−5081. (b) Ihmels, H.; Engels, B. B.; Faullhaber, K.; Lennartz, C. *Chem.—Eur. J.* **2000**, *6*, 2854−2864.
(56) Pascu, G. I.; Hotze, A. C. G.; Sanchez-Cano, C.; Kariuki, B. M.; Hannon, M. J. *Angew. Chem., Int. Ed.* **2007**, *46*, 4374−4378.
(57) Olmsted, J.; Kearns, D. R. *Biochemistry* **1977**, *16*, 3647−3654.
(58) (a) Boger, D. L.; Fink, B. E.; Brunette, S. R.; Tse, W. C.; Hedrick, M. P. *J. Am. Chem. Soc.* **2001**, *123*, 5878−5891. (b) Clever, G. H.; Söltl, Y.; Burks, H.; Spahl, W.; Carell, T. *Chem.—Eur. J.* **2006**, *12*, 8708−8718.
(59) Spiegel, K.; Magistrato, A. *Org. Biomol. Chem.* **2006**, *4*, 2507−2517.
(60) (a) Mahadevan, S.; Palaniandavar, M. *Inorg. Chem.* **1998**, *37*, 693−700. (b) Rajendiran, V.; Murali, M.; Suresh, E.; Palaniandavar, M.; Periasamy, V. S.; Akbarsha, M. A. *Dalton Trans.* **2008**, 2157−2170.
(61) Messori, L.; Orioli, P.; Tempi, C.; Marcon, G. *Biochem. Biophys. Res. Commun.* **2001**, *281*, 352−360.
(62) Schäfe, S.; Ott, I.; Gust, R.; Sheldrick, W. S. *Eur. J. Inorg. Chem.* **2007**, 3034−3046.
(63) Kumar, S.; Xue, L.; Arya, D. P. *J. Am. Chem. Soc.* **2011**, *133*, 7361−7375.
(64) Inohara, T.; Tarui, M.; Doi, M.; Inoue, M.; Ishida, T. *FEBS Lett.* **1993**, *324*, 301−304.
(65) Taima, H.; Okubo, A.; Yoshioka, N.; Inoue, H. *Chem.—Eur. J.* **2006**, *12*, 6331−6340.
(66) Brabec, V.; Nováková, O. *Drug Resist. Updates* **2006**, *9*, 111−122.
(67) (a) Zhang, W.; Yu, J.-S.; Liang, Y.; Fan, K.; Lai, L. *Spectrochim. Acta, Part A* **2004**, *60*, 2985−2992. (b) Roy, S.; Maheswari, P. U.; Lutz, M.; Spek, A. L.; den Dulk, H.; Barends, S.; Van Wezel, G. P.; Hartl, F.; Reedijk, J. *Dalton Trans.* **2009**, 10846−10860.
(68) Rajput, C.; Rutkaite, R.; Swanson, L.; Haq, I.; Thomas, J. A. *Chem.—Eur. J.* **2006**, *12*, 4611−4619.
(69) Childs, L. J.; Malina, J.; Rolfsnes, B. E.; Pascu, M.; Prieto, M. J.; Broome, M. J.; Rodger, P. M.; Sletten, E.; Moreno, V.; Rodger, A.; Hannon, M. J. *Chem.—Eur. J.* **2006**, *12*, 4919−4927.
(70) Staker, B. L.; Feese, M. D.; Cushman, M.; Pommier, Y.; Zembower, D.; Stewart, L.; Burgin, A. B. *J. Med. Chem.* **2005**, *48*, 2336−2345.
(71) (a) Wong, E. L.-M.; Fang, G.-S.; Che, C.-M.; Zhu, N. *Chem. Commun.* **2005**, 4578−4579. (b) Harrington, E. A.; Bruce, J. L.; Harlow, E.; Dyson, N. *Proc. Natl. Acad. Sci. U.S.A.* **1998**, *95*, 11945−11950. (c) Li, C. K.-L.; Sun, R. W.-Y.; Kui, S. C.-F.; Zhu, N.; Che, C.-M. *Chem.—Eur. J.* **2006**, *12*, 5253−5266.